Experimental Stress Separation Technique Using Thermoelasticity and Photoelasticity and Its Application to Fracture Mechanics*

Takahide SAKAGAMI**, Shiro KUBO**, Yasuyuki FUJINAMI*** and Yousuke KOJIMA**

This paper describes an experimental study on full-field stress separation from thermoelasticity and photoelasticity measurements and its application to estimation of stress intensity factor and the J-integral. Thermoelastic stress analysis (TSA) and photoelastic stress analysis (PSA) have been developed as full-field visualization methods of stress distribution. Only the sum of the principal stresses can be measured by TSA, while only the difference of the principal stresses can be measured by PSA. In this study, the hybrid stress separation measurement technique developed by the present authors using both of these methods was applied for determining distribution of all individual stress components in a center-cracked plate subjected to mechanical load. Stress intensity factor and the J-integral were calculated from the obtained stress distribution. In addition to the conventional calculation method, near-tip exclusive domain integral method was proposed, in which the J-integral was evaluated without using degraded experimental stress distribution data near the crack tip. It was found that these fracture mechanics parameters can be evaluated with good accuracies by the present technique.

Key Words: Thermoelasticity, Photoelasticity, Hybrid Technique, Stress Separation, Crack, Fracture Mechanics, Stress Intensity Factor, J-Integral

1. Introduction

Remarkable progress in numerical stress analyses such as the finite element method (FEM) and the boundary element method (BEM) enabled us to evaluate accurate stress distribution of loaded structural components even with complicated shapes. In the actual situations, however, we often encounter difficulties in conducting numerical stress analyses in actual components, because loading conditions or boundary conditions of the objective regions cannot be easily prescribed. Experimental techniques of stress evaluation are then very important. Thermoelastic stress measurement and photoelastic stress measurement have been widely used as full-field experimental stress evaluation methods. However these methods have limitations in the determination of individual stress components. Only the sum of the principal stresses can be determined by the thermoelastic stress measurement, while only the difference of the principal stresses can be determined by the photoelastic stress measurement. In order to solve this problem, many researchers have developed stress separation techniques[1)–5)]. Especially remarkable progress can be found in the development of stress separation techniques based on inverse analyses conducted by Murakami et al.[4] and Kishimoto et al.[5] In these techniques unknown boundary values were estimated by an inverse analysis using values of the sum of the principal stresses measured by thermoelastic method. A direct problem was solved to compute individual stress components using the boundary values determined by the inverse analysis. Kishimoto et al.[5] developed computational techniques to regularize the ill-posed inverse problems and improved the accuracy of the inverse analyses. Hayabusa et al.[6] proposed an improved stress separation technique based on the inverse problem using supplemental strain data obtained from strain gages.

Combined use of thermoelasticity and photoelasticity enables us to develop an experimental stress separation technique. Barone and Patterson[7] examined the practicability of the hybrid use of thermoelasticity and photo-

* Received 13th January, 2004 (No. 04-4013)

** Department of Mechanical Engineering and Systems, Graduate School of Engineering, Osaka University, 2–1 Yamadaoka, Suita, Osaka 565–0871, Japan.
E-mail: sakagami@mech.eng.osaka-u.ac.jp

*** Department of Mechanical Engineering and Systems, Graduate School of Engineering, Osaka University, Presently: Canon Inc., Tokyo, Japan

elasticity for obtaining the maximum and minimum principal stresses. In this study, the thermoelastic and photoelastic hybrid technique was developed for full-field separation measurement of the all individual stress components in plane-stress condition. First, stress separation of a loaded plate with a circular hole was investigated to show the feasibility of the proposed technique. Next, the proposed technique was applied to the stress separation measurement of a cracked plate to evaluate fracture mechanics parameters, such as stress intensity factors and the J-integral. For the J-integral calculation, near-tip exclusive domain integral method was proposed, in which the J-integral was evaluated without using degraded experimental stress distribution data near the crack tip.

2. Principle of Experimental Stress Separation Technique

2.1 Thermoelastic Stress Analysis (TSA)

Dynamic stress change causes very small temperature change under the adiabatic condition in solid. This phenomenon is called thermoelastic effect and is described by the following equation that relates temperature change (ΔT) to a change in the sum of the principal stresses ($\Delta\sigma$) under cyclic loading.

$$\Delta T = -\frac{\alpha}{\rho C_p} T \Delta\sigma \tag{1}$$

α : Coefficient of thermal expansion
ρ : Mass density
C_p : Specific heat at constant pressure
T : Absolute temperature

For measuring a very small thermoelastic temperature change, lock-in thermography with high resolution of temperature measurement is needed. The lock-in thermography correlates the load-induced infrared signal with the reference-loading signal enabling the noise reduction and the measurement of very small temperature changes due to the thermoelastic effect. As the lock-in thermography system, the infrared thermography with In-Sb array sensor (Raytheon Radiance HS) was employed with the lock-in data processor (Stress Photonics DeltaTherm 2000). Calibration relation between the sum of the principal stresses and the infrared radiation is required for obtaining the absolute stress values. In this experiment, calibration points, where uniform nominal stresses were supposed to be applied, were chosen on the specimen. The stress values calculated from the geometry of the employed specimen and the applied load were calibrated with the measured infrared radiation values.

2.2 Photoelastic Stress Analysis (PSA)

Coating photoelastic stress measurement system with a gray-field reflection polariscope (Stress Photonics PSA1000), which can measure the birefringence induced by strained plastic coatings installed on the specimen surface, was employed in this experiment. The rotating analyzer in the gray-field reflection polariscope analyzed the direction of the principal stress from the intensity of the transmitted light, which increased as the polarizer aligned with the major axis of the elliptical polarization and decreased as the polarizer aligned with its minor axis. Calibration relation between the difference of the principal stresses and the intensity of light is required for obtaining the absolute stress values. In this experiment, calibration points, where uniform nominal stresses were supposed to be applied, were again chosen on the specimen. The stress values calculated from the geometry of the employed specimen and the applied load were calibrated with the measured light intensity.

2.3 Stress separation by Mohr's stress circle

Mohr's stress circle can be drawn, as the sum of the principal stresses are determined by TSA, and the difference of the principal stresses and the direction of the principal stress are determined by PSA. All of the stress components can be determined from Mohr's stress circle.

3. Stress Measurement of a Plate with a Circular Hole

The feasibility of the present stress separation technique was evaluated by an experiment using a 2024 aluminum alloy plate specimen with a circular hole shown in Fig. 1. Thermoelastic stress measurement was carried out under cyclic tensile load. The maximum load and the minimum load were 2 940 N (19.6 MPa in nominal stress) and 0 N, respectively. The loading frequency was set to be 3 Hz. Thermoelastic stress measurement was carried out before photoelastic stress measurement, therefore no plastic coating for photoelastic stress measurement was applied during thermoelastic stress measurement. Only a flat black paint was applied to the specimen surface to keep high emissivity. Subsequently photoelastic stress measurement was carried out under the static tensile load of 2 940 N. The commercially available photoelastic coating (Measurement Group PS-1) was applied on the specimen surface. The area of stress separation was set in ACDF

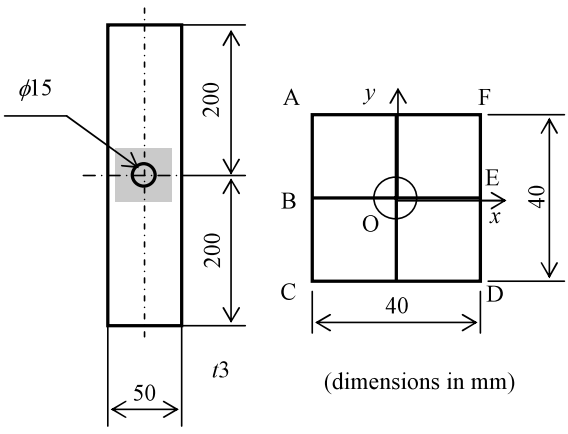

Fig. 1 Dimensions of specimen and area for stress separation

in Fig. 1. The sum of the principal stresses, the difference of the principal stresses and the direction of the principal stresses were obtained for 31×31 grid points in ACDF from TSA and PSA measurements, and the calculation of stress separation based on Mohr's stress circle was made at each grid point. Two-dimensional numerical analysis using the BEM was carried out for evaluating the accuracy of the present stress separation technique.

Distributions of the stress components σ_x, σ_y and τ_{xy} obtained by the present technique are shown in Fig. 2. The results of experimental stress separation are shown on the left hand side, and the BEM results are shown on the right hand side in Fig. 2. It is found that the experimentally obtained stress distributions agree with those computed by the BEM, demonstrating the feasibility of the present stress separation technique. Along the edge of the circular hole, however, the experimentally obtained stress values deviate from the actual values, due to the degraded accuracy of TSA by the edge effect. A slight difference is also found in the values of σ_x and σ_y on AF and FD. This is caused by the error in PSA. This makes measured differences of the principal stresses larger than actual values.

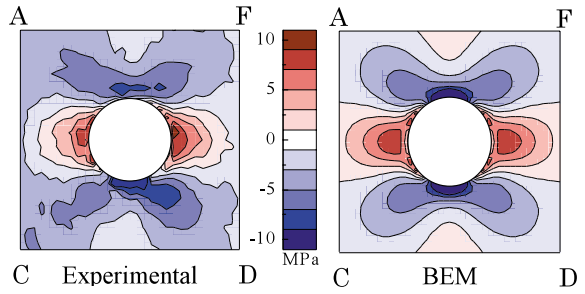

(a) Distribution of σ_x

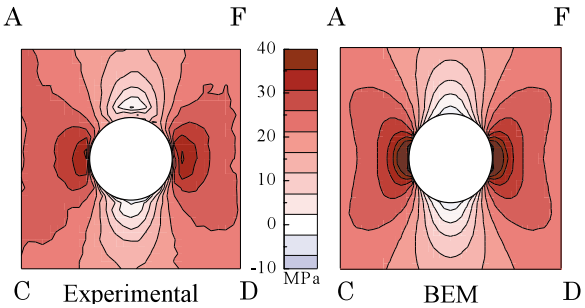

(b) Distribution of σ_y

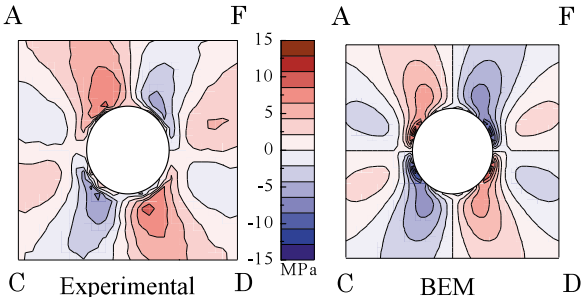

(c) Distribution of τ_{xy}

Fig. 2 Experimental result of stress separation for a specimen with a hole

4. Stress Measurement of a Plate with a Center Crack

An aluminum alloy plate specimen with a center crack, shown in Fig. 3, was employed for the experimental study. A through-thickness crack-like slit of 16 mm in length was introduced to the plate by electro-discharge machining. The width of the crack-like slit was 0.2 mm. Thermoelastic stress measurement was carried out under cyclic tensile load. The maximum load and the minimum load were 7 840 N (16.3 MPa in nominal stress) and 0 N, respectively. The loading frequency was 5 Hz. Photoelastic stress measurement was carried out under the static tensile load of 7 840 N. The area of stress separation was set in ACDF in Fig. 3. Two-dimensional BEM analysis was again carried out for evaluating the accuracy of stress separation. Quarter-point singular elements were used at the crack tip in the BEM analysis. The sum of the principal stresses, the difference of the principal stresses and the direction of the principal stresses were obtained for 80×200 grid points in ACDF from TSA and PSA measurement. The sum of the principal stresses measured by TSA system is shown in Fig. 4. The difference of the principal stresses obtained by PSA system is shown in Fig. 5. The experimental result is shown in the left hand side, and the BEM result is shown in the right hand side in the figures. It is found from Fig. 4 that the distribution of the sum of the principal stresses agrees very well with that calculated by the BEM analysis. It is found from Fig. 5 that obtained values of the difference of the principal stresses are a little smaller than those by the BEM analysis. Degradation of accuracy of PSA results may be attributed to the residual stresses in the specimen and the unsatisfactory installation of the photoelastic coating on the specimen.

The stress separation was conducted using the results of TSA and PSA measurement. Calculation of the stress separation was made at each grid point in ACDF. Ob-

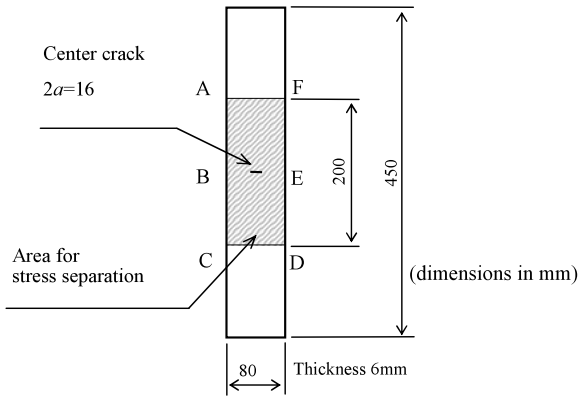

Fig. 3 Dimensions of specimen with a center crack

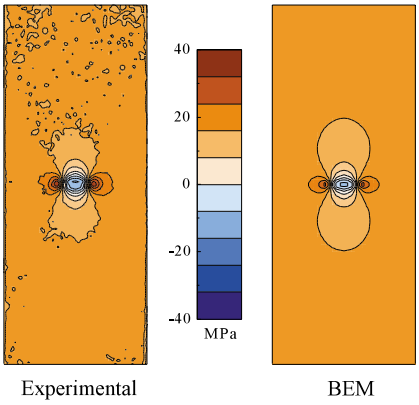

Fig. 4 Distribution of sum of principal stresses obtained by TSA measurement

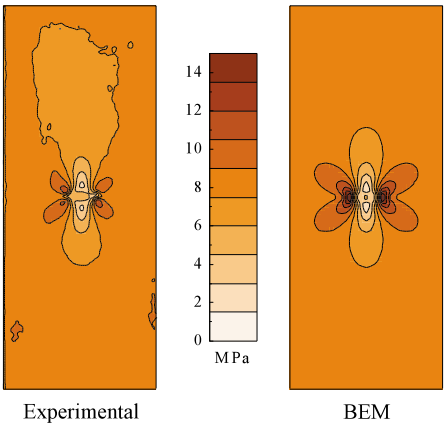

Fig. 5 Distribution of difference of principal stresses obtained by PSA measurement

tained distributions of the stress components σ_x, σ_y and τ_{xy} are shown in Fig. 6. The experimental stress separation result is shown in the left hand side, and the BEM result is shown in the right hand side in Fig. 6. It is found that the stress distributions obtained by the experimental stress separation agree with those computed by the BEM analyses. Slight differences are found near the crack tip between experimental stress values and numerical ones. This is due to the experimental error in PSA measurement as described in the foregoing paragraph.

5. Experimental Evaluation of Fracture Mechanics Parameters

Fracture mechanics parameters were calculated using the individual stress components obtained by the present stress separation technique.

5.1 Stress intensity factor

First, mode I stress intensity factor K_{I} was calculated based on the stress extrapolation method. Under the mode I loading, σ_y near the crack tip is given as the following equation using the coordinate system shown in Fig. 7.

$$\sigma_y = \frac{K_{\mathrm{I}}}{\sqrt{2\pi r}} \cos\frac{\theta}{2}\left(1+\sin\frac{\theta}{2}\sin\frac{3\theta}{2}\right) \qquad (2)$$

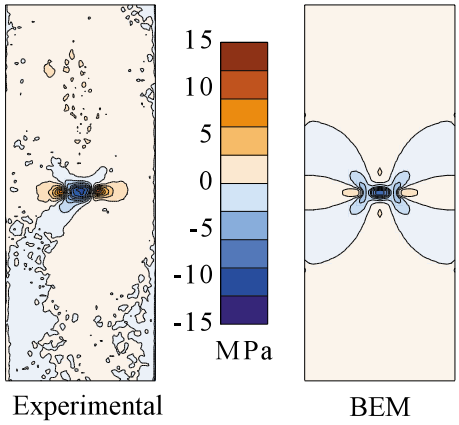

(a) Distribution of σ_x

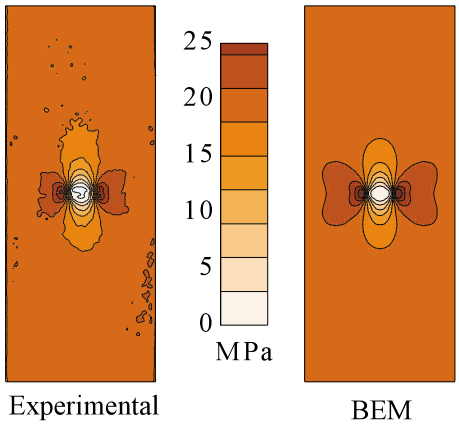

(b) Distribution of σ_y

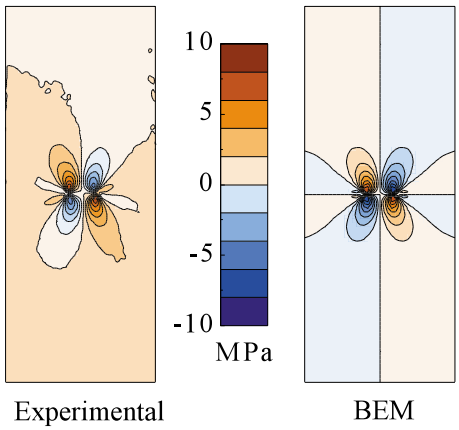

(c) Distribution of τ_{xy}

Fig. 6 Experimental result of stress separation for a specimen with a center crack

K_{I} can be determined by the following equation extrapolating the σ_y value along the line in front of the crack tip ($\theta = 0$).

$$K_{\mathrm{I}} = \lim_{r\to 0} \sqrt{2\pi r}\,\sigma_y|_{\theta=0} \qquad (3)$$

Calculated value of K_{I} is shown in Table 1, as well as the theoretically obtained value[8]. It is found that K_{I} value can be evaluated from experimentally obtained stress distribution with the error less than 5%.

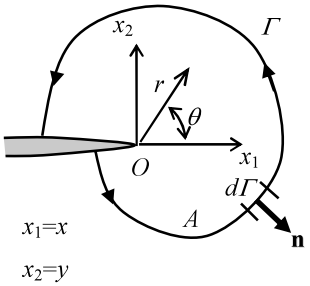

Fig. 7 A coordinate near the crack tip and J-integral path

Table 1 Estimation of stress intensity factor

	K_1(MPa$\sqrt{\text{m}}$)	Error %
Experimental Value	2.778	4.7
Exact Value	2.653	

5.2 J-integral by line integral method

The J-integral was evaluated based on the path integral method. The J-integral is given as the following line integral along an arbitrary counterclockwise path Γ surrounding the crack tip shown in Fig. 7.

$$J=\int_{\Gamma}\left(Wn_1-T_i\frac{\partial u_i}{\partial x_1}\right)d\Gamma \tag{4}$$

where W is the strain energy density, n_1 is x_1-component of unit normal vector $\boldsymbol{n}$, and T_i is traction on Γ. Numerical integration was carried out along Γ using individual stress values obtained by the stress separation. In Eq. (4), $\partial u_2/\partial x_1$ cannot be directly obtained by the present stress separation technique. Therefore, it was assumed that u_2 takes a uniform value on AF and CD, and u_2 on the integral path was determined by integrating the strain value in the x_2-direction based on the uniform value of u_2.

The J-integral was obtained for 176 different paths around the crack tip. Square paths were selected as path Γ combining lines parallel to the x_1- and x_2-axis as shown in Fig. 8. Segment of path Γ parallel to the y-axis was taken along the lines $x_1=a$ and $x_1=b$. Segment of path Γ parallel to the x-axis was taken along the lines $x_2=100$ mm and $x_2=-100$ mm. By the combinations of a and b, 176 square paths were defined.

The J-integral values obtained from experimental stress separation data are shown in Table 2, as well as the theoretical value obtained from the stress intensity factor K_{I}. It is found that J value can be evaluated from experimentally obtained stress distribution accurately based on the line integral method. It is also found in the table that the accuracy of the J-integral value was improved when the line integral paths were set in a remote area from crack tips.

5.3 J-integral by domain integral method

The J-integral based on the domain integral method was proposed for the J-integral calculation using numerical data on stress distribution around crack[9]. The J-integral is given by the following equation for domain A surrounded by boundary Γ, provided that no force was applied on the crack face.

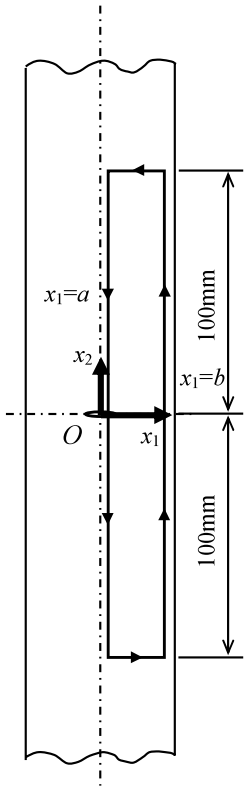

Fig. 8 Integral path used for calculating of J-integral by line integral method

Table 2 Estimation of the J-integral by line integral

		a (mm)						
		-5	-3	-1	0	1	3	5
b (mm)	15	85.27	86.13	91.81	95.42	93.45	87.82	85.90
		11.4	10.5	4.6	0.9	2.9	8.8	10.8
	20	85.81	86.67	92.36	95.96	93.99	88.37	86.44
		10.9	10.0	4.1	0.3	2.4	8.2	10.2
	25	87.41	88.27	93.95	97.56	95.58	89.96	88.03
		9.2	8.3	2.4	1.3	0.7	6.6	8.6
	30	89.73	90.59	96.27	99.88	97.90	92.28	90.35
		6.8	5.9	0.0	3.8	1.7	4.1	6.1
								J (J/m^2)
Exact Value: J = 96.27								Error (%)

$$J=\int_A\left\{\left(-W\delta_{1j}+\sigma_{ij}u_{i,1}\right)q_{,j}+\left(-W_{,1}+\sigma_{ij}\varepsilon_{ij,1}\right)q\right\}dA, \tag{5}$$

where q is an arbitrary variable defined in the domain A which satisfies the following equations.

$$\begin{cases} q=1 & \text{at crack tip} \\ q=0 & \text{on } \Gamma \end{cases} \tag{6}$$

In this study, the J-integral was calculated for the elliptical domain with minor axis a and major axis b, whose center coincides with the crack tip $\boldsymbol{O}(O_x,O_y)$. The variable q given by the following equation was employed for the elliptical domain integral.

Table 3 Estimation of the J-integral by domain integral

		b (mm)				
		20	30	40	50	60
a (mm)	5	67.59	67.92	68.65	69.08	69.12
		29.8	29.4	28.7	28.2	28.2
	7	74.02	74.66	75.45	75.89	76.09
		23.1	22.4	21.6	21.2	21.0
	9	77.14	77.93	78.85	79.33	79.63
		19.9	19.0	18.1	17.6	17.3
	11	78.65	79.84	80.90	81.51	81.83
		18.3	17.1	16.0	15.3	15.0
	13	79.93	81.38	82.74	83.50	83.80
		17.0	15.5	14.1	13.3	13.0
						J (J/m^2)
Exact Value: $J = 96.27$						Error (%)

$$q(x,y) = 1 - \left\{ \frac{(x-O_x)^2}{a^2} + \frac{(y-O_y)^2}{b^2} \right\} \tag{7}$$

The numerical integration was carried out for 25 different domains using individual stress values obtained by the stress separation. The calculated J-integral values are shown in Table 3, as well as the theoretical value. It is found that J-integral values evaluated from experimentally obtained stress distribution were degraded compared with those by the line integral method.

5.4 J-integral by near-tip exclusive domain integral method

It was shown in the foregoing paragraph that the J-integral by the domain integral method was effectively employed for the experimental evaluation of the J-integral. However the accuracy of the J-integral evaluation was degraded compared with that of the line-integral method, even though the same individual stress values obtained by the stress separation were used. This seems to be caused by the fact that error in the experimentally obtained stress values was large near the crack tip where the stress values showed steep distribution.

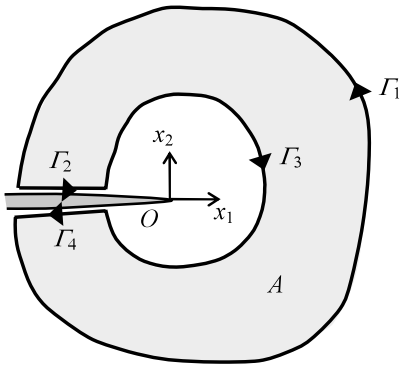

Fig. 9 Near-tip exclusive domain A for the J-integral

To take the both benefits of the line-integral method and the domain-integral method, the near-tip exclusive domain integral method is newly proposed for the J-integral evaluation. Near-tip region where a error is expected in the experimentally obtained stress values is removed to make a near-tip exclusive domain for the J-integral evaluation as shown in Fig. 9. Near-tip exclusive domain A is defined by the surrounding closed path $\Gamma = \Gamma_1 + \Gamma_2 + \Gamma_3 + \Gamma_4$. The J-integral for path Γ_1 can be given as the following equation.

$$J_{\Gamma_1} = \int_{\Gamma_1} \left(W n_1 - \sigma_{ij} n_j \frac{\partial u_i}{\partial x_1} \right) d\Gamma \tag{8}$$

Multiplying the integrand by a differentiable function q, taking integration over a closed path $\Gamma_1 + \Gamma_2 + \Gamma_3 + \Gamma_4$ and applying Green formula, the following equation is obtained.

$$\int_{\Gamma_1+\Gamma_2+\Gamma_3+\Gamma_4} \left(W n_1 - \sigma_{ij} n_j \frac{\partial u_i}{\partial x_1} \right) q d\Gamma = \int_A \left[\frac{\partial}{\partial x_1}(Wq) - \frac{\partial}{\partial x_j}\left(\sigma_{ij} \frac{\partial u_i}{\partial x_1} q \right) \right] dA$$

$$= \int_A \left(\frac{\partial W}{\partial x_1} q + W \frac{\partial q}{\partial x_1} - \frac{\partial \sigma_{ij}}{\partial x_j} \frac{\partial u_i}{\partial x_1} q - \sigma_{ij} \frac{\partial^2 u_i}{\partial x_1 \partial x_j} q - \sigma_{ij} \frac{\partial u_i}{\partial x_1} \frac{\partial q}{\partial x_j} \right) dA \tag{9}$$

In Eq. (9), $\partial W / \partial x_1$ can be written as,

$$\frac{\partial W}{\partial x_1} = \frac{\partial W}{\partial \varepsilon_{ij}} \frac{\partial \varepsilon_{ij}}{\partial x_1} = \frac{\sigma_{ij}}{2} \left(\frac{\partial^2 u_i}{\partial x_1 \partial x_j} + \frac{\partial^2 u_j}{\partial x_1 \partial x_i} \right) = \sigma_{ij} \frac{\partial^2 u_i}{\partial x_1 \partial x_j}. \tag{10}$$

Invoking the equilibrium condition,

$$\frac{\partial \sigma_{ij}}{\partial x_j} = 0, \tag{11}$$

and Eq. (10), the right-hand side of Eq. (9) can be written as,

$$\int_A \left[W \frac{\partial q}{\partial x_1} - \sigma_{ij} \frac{\partial u_i}{\partial x_1} \frac{\partial q}{\partial x_j} \right] dA. \tag{12}$$

Defining the arbitrary variable q which satisfies that $q = 1$ on Γ_1 and $q = 0$ on Γ_3, the left-hand side of Eq. (9) can be written as,

$$\int_{\Gamma_1} \left(W n_1 - \sigma_{ij} n_j \frac{\partial u_i}{\partial x_1} \right) q d\Gamma, \tag{13}$$

since $n_1 = 0$ and $T_i = 0$ on Γ_2 and Γ_4. Therefore, the J-integral for near-tip exclusive domain can be given by the following equation.

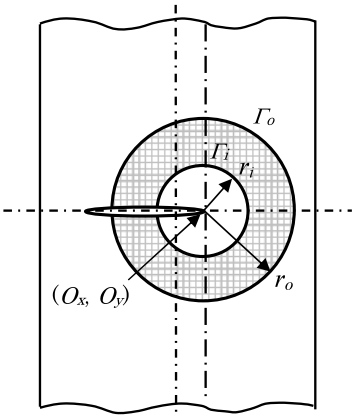

Fig. 10 Near tip exclusive domain employed for the J-integral by domain integral method

$$J_{\Gamma_1}=\int_{\Gamma}\left(Wn_1-\sigma_{ij}n_j\frac{\partial u_i}{\partial x_1}\right)d\Gamma$$
$$=\int_{\Gamma_1}\left(Wn_1-\sigma_{ij}n_j\frac{\partial u_i}{\partial x_1}\right)qd\Gamma$$
$$=\int_A\left[W\frac{\partial q}{\partial x_1}-\sigma_{ij}\frac{\partial u_i}{\partial x_1}\frac{\partial q}{\partial x_j}\right]dA \qquad (14)$$
$$\begin{cases} q=1 & \text{on}\,\Gamma_1 \\ q=0 & \text{on}\,\Gamma_3 \end{cases}$$

The J-integral was evaluated for the near tip exclusive domain defined as the donut-like inter area between two circles as shown in Fig. 10. Then the arbitrary variable q was defined by the following equation.

$$q(x,y)=\frac{r_o^2-\{(x-O_x)^2+(y-O_y)^2\}}{r_o^2-r_i^2} \qquad (15)$$
$$\begin{cases} q=1 & \text{on inner boundary}\,\Gamma_i \\ q=0 & \text{on outer boundary}\,\Gamma_o \end{cases}$$

The numerical integration was carried out for 104 different near tip exclusive donut-like domains defined by the combinations of r_i and r_o using individual stress values obtained by the stress separation. Obtained J values are shown in Table 4, as well as the theoretical value. It is found that J value can be evaluated accurately from experimentally obtained stress distribution demonstrating the effectiveness of the present near tip exclusive domain integral method. The accuracy of the J-integral was improved when the donut-like inter area between two circles was set at the distant area from the crack tip and the width of the donut-like area was relatively narrow.

6. Conclusions

In this study, the thermoelastic and coating photoelastic hybrid technique was developed for full-field separation measurement of all the individual stress components. Stress separation of a loaded plate with a circular hole can be conducted with good accuracy demonstrating the feasibility of the proposed technique. Furthermore, the proposed technique was applied to the stress separation measurement of a cracked plate. Fracture mechanics parameters, i.e., stress intensity factor and the J-integral were evaluated. For the J-integral calculation, near-tip exclusive domain integral method was newly proposed. It was found that fracture mechanics parameters were accurately evaluated using the obtained stress distributions.

Table 4 Evaluation of the J-integral by near-tip exclusive domain integral

		r_o-r_i (mm)				
		1	2	3	4	5
r_o (mm)	6	83.06	82.42	81.59	79.37	76.68
		13.7	14.4	15.2	17.6	20.3
	8	85.12	84.52	84.03	83.58	83.03
		11.6	12.2	12.7	13.2	13.8
	10	87.16	86.73	86.21	85.72	85.29
		9.5	9.9	10.4	11.0	11.4
	12	90.23	89.34	88.59	88.09	87.60
		6.3	7.2	8.0	8.5	9.0
	14	89.70	90.29	90.26	89.84	89.35
		6.8	6.2	6.2	6.7	7.2
						J (J/m^2)
Exact Value: J = 96.27						Error (%)

References

(1) Ryall, T.G. and Wong, A.K., Determining Stress Components from Thermoelastic Data — A Theoretical Study, Mechanics of Materials, Vol.7 (1986), pp.205–214.

(2) Huang, Y.M., Rowlands, R.E. and Lesniak, J.R., Simultaneous Stress Separation, Smoothing of Measured Thermoelastic Isopachic Information and Enhanced Boundary Data, Experimental Mechanics, Vol.30 (1990), pp.398–403.

(3) Feng, Z., Zhang, D., Rowlands, R.E. and Sandor, B.I., Thermoelastic Determination of Individual Stress Components in Loaded Composites, Experimental Mechanics, Vol.32 (1992), pp.89–95.

(4) Murakami, Y. and Yoshimura, M., Development of System Resolving All Stress Components in Thermoelastic Stress Analysis, Trans. Jpn. Soc. Mech. Eng., (in Japanese), Vol.61, No.591 (1995), pp.2482–2488.

(5) Kishimoto, K., Inoue, H., Shinbo, H. and Shibuya, T., Inverse Analysis Related to Stress Separation in Thermoelastic Stress Analysis, JSME Int. J., Ser. A., Vol.40, No.2 (1997), pp.108–116.

(6) Hayabusa, K., Inoue, H., Kishimoto, K. and Shibuya, T., Boundary Element Inverse Analysis for Stress Separation in Thermoelastic Stress Analysis, JSME Int. J., Ser. A., Vol.42, No.4 (1999), pp.618–623.

(7) Barone, S. and Patterson, E.A., Full-Field Separation of Principal Stresses by Combined Thermo- and Photoelasticity, Experimental Mechanics, Vol.36 (1996), pp.318–324.

(8) Tada, H., Paris, P.C. and Irwin, G.R., Stress Analysis of Cracks Handbook, (1973), Del Research Corp.

(9) Moran, B. and Shih, C.F., Crack Tip and Associated Domain Integrals from Momentum and Energy Balance, Engineering Fracture Mechanics, Vol.27, No.6 (1987), pp.615–642.